Available online at www.sciencedirect.com
SCIENCE DIRECT®
Comput. Methods Appl. Mech. Engrg. 195 (2006) 2209–2230
Computer methods in applied mechanics and engineering
www.elsevier.com/locate/cma

Non-linear strain–displacement equations exactly representing large rigid-body motions. Part II. Enhanced finite element technique

G.M. Kulikov *, S.V. Plotnikova

Department of Applied Mathematics and Mechanics, Tambov State Technical University, Sovetskaya Street, 106, Tambov 392000, Russia

Received 5 February 2004; received in revised form 22 November 2004; accepted 4 May 2005

Abstract

The precise representation of arbitrarily large rigid-body motions in the displacement patterns of curved Timoshenko–Mindlin-type (TM) shell elements has been considered in Part I of the present work. This consideration required the development of strain–displacement equations of the finite deformation TM shell theory, written in local curvilinear coordinates, with regard to their consistency with the large rigid-body motions. For this purpose the displacement vectors of the face surfaces are introduced and resolved in the reference surface frame. In this paper economical schemes of evaluating the stiffness matrix by means of the analytical integration inside the element and an advanced approach for solving incremental equilibrium equations are discussed in detail. The developed approach may allow the use of load increments that are much larger than possible with the approach proposed in Part I. The numerical results are presented to demonstrate the high accuracy and effectiveness of the developed four-node curved shell elements and to compare their performance with non-linear solid-shell elements extracted from the literature.

Keywords: First-order multilayered shell theory; Finite deformation; Four-node curved shell elements; Assumed stress–strain formulation

* Corresponding author. Fax: +7 075 253 2017.
E-mail address: kulikov@apmath.tstu.ru (G.M. Kulikov).
URL: http://apm.tstu.ru/kulikov (G.M. Kulikov).

0045-7825/$ - see front matter
doi:10.1016/j.cma.2005.05.006

1. Introduction

One of the main requirements of the modern first-order shell theory that is intended for the general non-linear finite element (FE) formulation is that it must lead to strain-free modes for arbitrarily large rigid-body motions. The adequate representation of large rigid-body motions is a necessary condition if a non-linear element is to have the good accuracy and convergence properties. Therefore, when an inconsistent non-linear shell theory is used to construct any finite element, erroneous straining modes under arbitrarily large rigid-body motions may be appeared. This problem has been studied for the finite deformation Timoshenko beam, Mindlin plate and Timoshenko–Mindlin-type (TM) shell theories in Refs. [1–3]. In these theories displacements of the bottom and top surfaces are introduced in order to exactly describe rigid-body motions.

It is common knowledge that in some works developing the solid-shell concept [4–7] displacement vectors of the face surfaces of the shell are also used and represented in some global Cartesian basis to precisely describe large rigid-body motions. But in the TM shell theory [3] selecting as unknowns displacements of the bottom and top surfaces has a principally another mechanical sense and allows one to formulate any four-node *curved* shell element on the basis of the non-linear strain–displacement relationships, written in local curvilinear coordinates, which are objective, i.e., invariant under all rigid-body motions. Taking into account that displacement vectors of the face surfaces are resolved in the *reference surface frame*, the developed FE formulation has computational advantages compared to the conventional isoparametric FE formulations, since it reduces the costly numerical integration by deriving the elemental stiffness matrices. It is remarkable that element matrices require only direct substitutions, i.e., no inversion is needed when sides of the element coincide with the lines of principal curvatures of the reference surface, and they are evaluated by using the *analytical integration*.

It should be mentioned that a close 6-parameter shell model was proposed by Simo et al. [8] where covariant derivatives, associated with the Riemannian connection on the reference surface, do not explicitly appear in the formulation. The advantage of the 6-parameter shell formulation [8] compared to the 5-parameter one is that the thickness stretch plays an important role in many engineering problems such as concentrated surface loading, contact and delamination of composite shells. An essential feature of our geometrically exact shell FE model is that, in contrast with Ref. [8], Christoffel symbols and coefficients of the second fundamental form appear in the formulation. This clears the way to elaborate in conjunction with the incremental total Lagrangian formulation the more robust numerical algorithms. The main reason is that during the geometrical modeling in CAD systems the surfaces are usually generated by non-uniform rational B-spline (NURBS) functions [9]. So, exact NURBS shell surface functions may be directly used for describing the reference surface that would yield an efficient numerical implementation, which will be free from mathematical complexities and suitable for large scale computations.

Herein, it is developed a refined FE formulation compared to Ref. [3] that is based on the simple and efficient approximation of TM shells via four-node curved elements. To overcome shear and membrane locking and have no spurious zero energy modes, the assumed strain and stress resultant fields are invoked. This approach may be treated as an assumed stress–strain formulation and was proposed by Wempner et al. [10] for the geometrically linear TM shell without the thickness change. In order to circumvent thickness locking, modified material stiffness matrices symmetric [11–14] or non-symmetric [1–3,15,16] corresponding to the generalized plane stress state may be employed. In the present paper the second (more general) approach is used. The fundamental unknowns consist of six displacements and 11 strains of the face surfaces of the shell, and 11 stress resultants. Therefore, for deriving governing FE equations the Hu–Washizu variational principle should be applied.

The FE formulation developed in Part I [3] is free of assumptions of small displacements, small rotations and small loading steps because it is based on the objective *fully* non-linear strain–displacement relationships. There exists only one limitation associated with a simple fact that a loading step cannot be too large.

This restriction arises in case of using the Newton–Raphson method for solving equilibrium equations for incremental nodal degrees of freedom, i.e., in Part I the incremental assumed strains and stress resultants are eliminated at the element level. Herein, it is discussed an alternative approach when equilibrium equations for incremental displacements and incremental assumed strains and stress resultants are solved by the Newton–Raphson method *simultaneously*. As a result an additional incremental load vector due to so-called compatibility mismatch [7,12,17–19] is present and disappears at the end of the iteration process. So, this enhanced approach allows, as a rule, to use much larger load increments in comparison with Part I.

The numerical results are presented to demonstrate the efficiency and high accuracy of both developed approaches and to compare their with other non-linear state-of-the-art FE formulations. For this purpose extensive numerical studies are employed.

2. Preliminaries

Consider a shell built up in the general case by the arbitrary superposition across the wall thickness of N layers of uniform thickness h_k. The kth layer may be defined as a 3D body of volume V_k bounded by two surfaces S_{k-1} and S_k, located at the distances δ_{k-1} and δ_k measured with respect to the reference surface S, and the edge boundary surface Ω_k (see Fig. 1). The full edge boundary surface $\Omega = \Omega_1 + \Omega_2 + \cdots + \Omega_N$ is generated by the normals to the reference surface along the bounding curve Γ (with the arc length s) of this surface. It is also assumed that the bounding surfaces S_{k-1} and S_k are continuous, sufficiently smooth and without any singularities. Let the reference surface S be referred to the orthogonal curvilinear coordinate system α_1 and α_2, which coincides with the lines of principal curvatures of its surface, whereas coordinate α_3 is oriented along the unit vector $\boldsymbol{a}_3 = \mathbf{e}_3$ normal to the reference surface; $\boldsymbol{a}_\alpha = A_\alpha \mathbf{e}_\alpha$ are the basis vectors of the reference surface S; $\mathbf{g}_\alpha^\pm = A_\alpha^\pm \mathbf{e}_\alpha$ are the basis vectors of the face surfaces $S^\pm$; $\mathbf{e}_\alpha$ are the tangent unit vectors to the lines of principal curvatures of the reference surface; A_α and $A_\alpha^\pm$ are the Lamé coefficients of the reference and face surfaces.

The constituent layers of the shell are supposed to be rigidly joined, so that no slip on contact surfaces and no separation of layers can occur. The material of each constituent layer is assumed to be linearly

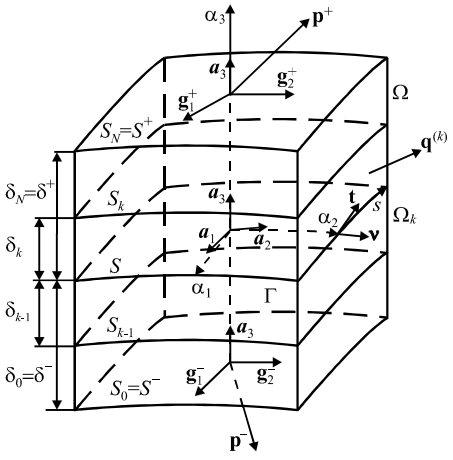

Fig. 1. Multilayered shell element.

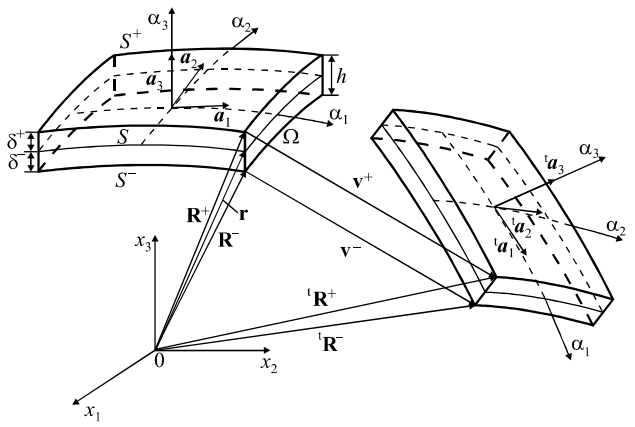

Fig. 2. Geometry and kinematics of shell: (a) initial configuration and (b) current configuration.

elastic, anisotropic, homogeneous or fiber reinforced, such that in each point there is a single surface of elastic symmetry parallel to the reference surface. Let p_i^- and p_i^+ be the components of the external loading vectors $\mathbf{p}^-$ and $\mathbf{p}^+$ acting on the bottom surface $S^- = S_0$ and top surface $S^+ = S_N$ in the α_i coordinate directions; $\mathbf{q}^{(k)} = q_v^{(k)}\mathbf{v} + q_t^{(k)}\mathbf{t} + q_3^{(k)}\mathbf{e}_3$ be the external loading vector acting on the edge boundary surface Ω_k, where $q_v^{(k)}$, $q_t^{(k)}$ and $q_3^{(k)}$ are the components of its vector in the v, t and α_3 directions; $\mathbf{v}$ and $\mathbf{t}$ are the normal and tangential unit vectors to the bounding curve Γ (see Fig. 1). Here and in the following developments the index k identifies the belonging of any quantity to the kth layer and runs from 1 to N; the abbreviation $(\,)_{,\alpha}$ implies the partial derivatives with respect to the coordinate α_1 and α_2; indices i, j, ℓ, m take the values 1, 2 and 3 while Greek indices α, β, γ, δ take the values 1 and 2.

The finite deformation TM shell theory is based on the linear approximation of displacements in the thickness direction

$$ {}^t\mathbf{R} = N^-(\alpha_3)\,{}^t\mathbf{R}^- + N^+(\alpha_3)\,{}^t\mathbf{R}^+, \quad {}^t\mathbf{R}^\pm = \mathbf{R}^\pm + \mathbf{v}^\pm, \quad \mathbf{R}^\pm = \mathbf{r} + \delta^\pm \mathbf{e}_3, \tag{1a} $$

$$ \mathbf{v}^\pm = \sum_i v_i^\pm \mathbf{e}_i, \tag{1b} $$

$$ N^-(\alpha_3) = \frac{1}{h}(\delta^+ - \alpha_3), \quad N^+(\alpha_3) = \frac{1}{h}(\alpha_3 - \delta^-), \tag{1c} $$

where $\mathbf{r}(\alpha_1, \alpha_2)$ is the position vector of the reference surface; $\mathbf{R}^\pm$ are the position vectors of the face surfaces in the initial shell configuration; $\mathbf{v}^\pm$ are the displacement vectors of the face surfaces; $v_i^\pm(\alpha_1, \alpha_2)$ are the components of these vectors, which are always measured in accordance with the total Lagrangian formulation from the initial configuration to the current configuration directly (see Fig. 2); $N^\pm(\alpha_3)$ are the linear through-the-thickness shape functions; h is the thickness of the shell. It is important that displacement vectors (1b) are represented in the orthonormal reference surface basis $\mathbf{e}_i$ that allows one to reduce the costly numerical integration by deriving the elemental stiffness matrix.

3. Strain–displacement relationships

The strain–displacement relationships of the finite deformation TM shell theory [3] can be rewritten in a more convenient form for the FE implementation as

$$\varepsilon^{DS}_{\alpha\beta} = N^{-}(\alpha_3)\mathscr{E}^{-}_{\alpha\beta} + N^{+}(\alpha_3)\mathscr{E}^{+}_{\alpha\beta}, \tag{2a}$$

$$\varepsilon^{DS}_{\alpha 3} = N^{-}(\alpha_3)\mathscr{E}^{-}_{\alpha 3} + N^{+}(\alpha_3)\mathscr{E}^{+}_{\alpha 3}, \tag{2b}$$

$$\varepsilon^{DS}_{33} = \mathscr{E}_{33}. \tag{2c}$$

Here, $\mathscr{E}^{\pm}_{\alpha\beta}$ and $\mathscr{E}^{\pm}_{\alpha 3}$ are the tangential and transverse shear components of the Green–Lagrange strain tensor of face surfaces $S^{\pm}$ defined by

$$2\mathscr{E}^{\pm}_{\alpha\beta} = \frac{1}{A_\alpha A_\beta}({}^t\mathbf{g}^{\pm}_\alpha \cdot {}^t\mathbf{g}^{\pm}_\beta - \mathbf{g}^{\pm}_\alpha \cdot \mathbf{g}^{\pm}_\beta) = \frac{\zeta^{\pm}_\beta}{A_\alpha}\mathbf{v}^{\pm}_{,\alpha}\cdot\mathbf{e}_\beta + \frac{\zeta^{\pm}_\alpha}{A_\beta}\mathbf{v}^{\pm}_{,\beta}\cdot\mathbf{e}_\alpha + \frac{1}{A_\alpha A_\beta}\mathbf{v}^{\pm}_{,\alpha}\cdot\mathbf{v}^{\pm}_{,\beta}, \tag{3a}$$

$$2\mathscr{E}^{\pm}_{\alpha 3} = \frac{1}{A_\alpha}({}^t\mathbf{g}^{\pm}_\alpha \cdot {}^t\boldsymbol{a}_3 - \mathbf{g}^{\pm}_\alpha \cdot \boldsymbol{a}_3) = \zeta^{\pm}_\alpha\boldsymbol{\beta}\cdot\mathbf{e}_\alpha + \frac{1}{A_\alpha}\mathbf{v}^{\pm}_{,\alpha}\cdot(\mathbf{e}_3+\boldsymbol{\beta}), \tag{3b}$$

$$2\mathscr{E}_{33} = {}^t\boldsymbol{a}_3\cdot{}^t\boldsymbol{a}_3 - \boldsymbol{a}_3\cdot\boldsymbol{a}_3 = 2\boldsymbol{\beta}\cdot\left(\mathbf{e}_3 + \frac{1}{2}\boldsymbol{\beta}\right), \tag{3c}$$

$${}^t\mathbf{g}^{\pm}_\alpha = {}^t\mathbf{R}^{\pm}_{,\alpha} = \mathbf{g}^{\pm}_\alpha + \mathbf{v}^{\pm}_{,\alpha}, \quad \mathbf{g}^{\pm}_\alpha = \mathbf{R}^{\pm}_{,\alpha} = A^{\pm}_\alpha\mathbf{e}_\alpha, \quad {}^t\boldsymbol{a}_3 = \boldsymbol{a}_3 + \boldsymbol{\beta}, \tag{3d}$$

$$\boldsymbol{\beta} = \frac{1}{h}(\mathbf{v}^{+} - \mathbf{v}^{-}), \quad A^{\pm}_\alpha = A_\alpha\zeta^{\pm}_\alpha, \quad \zeta^{\pm}_\alpha = 1 + k_\alpha\delta^{\pm},$$

where k_α are the principal curvatures of the reference surface. Strain–displacement relationships (2) and (3) are very attractive because they are objective, i.e., invariant under arbitrarily large rigid-body motions. A proof of this statement may be obtained by using a technique [3]. The advantage of relations (3a) and (3b) compared to those reported in Part I is that parameters $\zeta^{\pm}_\alpha$ characterizing curvatures of the face surfaces do not appear in *non-linear* terms.

Further we prove a fundamental result concerning a link between transverse components of the Green–Lagrange strain tensor (2) that was not presented in Part I.

Proposition. *The transverse components of the Green–Lagrange strain tensor of the TM shell theory satisfy the following linking conditions*:

$$2(\mathscr{E}^{+}_{\alpha 3} - \mathscr{E}^{-}_{\alpha 3}) = \frac{1}{A_\alpha}h\mathscr{E}_{33,\alpha}. \tag{4}$$

Proof. Using Eqs. (3b) and (3d) yields

$$2(\mathscr{E}^{+}_{\alpha 3} - \mathscr{E}^{-}_{\alpha 3}) = \frac{1}{A_\alpha}h[A_\alpha k_\alpha\boldsymbol{\beta}\cdot\mathbf{e}_\alpha + \boldsymbol{\beta}_{,\alpha}\cdot(\mathbf{e}_3+\boldsymbol{\beta})]. \tag{5}$$

Taking into account well-known formulas for derivatives of the basis vectors with respect to the orthogonal curvilinear coordinates α_1 and α_2 [20], one obtains from Eq. (3c)

$$\mathscr{E}_{33,\alpha} = \boldsymbol{\beta}\cdot\mathbf{e}_{3,\alpha} + \boldsymbol{\beta}_{,\alpha}\cdot(\mathbf{e}_3+\boldsymbol{\beta}) = A_\alpha k_\alpha\boldsymbol{\beta}\cdot\mathbf{e}_\alpha + \boldsymbol{\beta}_{,\alpha}\cdot(\mathbf{e}_3+\boldsymbol{\beta}). \tag{6}$$

Required relation (4) immediately follows from Eqs. (5) and (6). □

Finally, we represent strain–displacement relationships (3) in a scalar form as

$$\mathscr{E}^{\pm}_{\alpha\beta} = e^{\pm}_{\alpha\beta} + \eta^{\pm}_{\alpha\beta}, \quad \mathscr{E}^{\pm}_{\alpha 3} = e^{\pm}_{\alpha 3} + \eta^{\pm}_{\alpha 3}, \quad \mathscr{E}_{33} = e_{33} + \eta_{33}. \tag{7}$$

Here, $e^{\pm}_{\alpha\beta}$, $e^{\pm}_{\alpha 3}$, e_{33} and $\eta^{\pm}_{\alpha\beta}$, $\eta^{\pm}_{\alpha 3}$, η_{33} are the linear and non-linear components of the Green–Lagrange strain tensor defined by

$$e^{\pm}_{\alpha\alpha} = \zeta^{\pm}_{\alpha}\lambda^{\pm}_{\alpha}, \quad 2e^{\pm}_{12} = \zeta^{\pm}_{2}\omega^{\pm}_{1} + \zeta^{\pm}_{1}\omega^{\pm}_{2}, \quad 2e^{\pm}_{\alpha 3} = \zeta^{\pm}_{\alpha}\beta_{\alpha} - \theta^{\pm}_{\alpha}, \quad e_{33} = \beta_3, \tag{8a}$$

$$\eta^{\pm}_{\alpha\alpha} = \tfrac{1}{2}[(\lambda^{\pm}_{\alpha})^2 + (\omega^{\pm}_{\alpha})^2 + (\theta^{\pm}_{\alpha})^2], \quad 2\eta^{\pm}_{12} = \lambda^{\pm}_{1}\omega^{\pm}_{2} + \lambda^{\pm}_{2}\omega^{\pm}_{1} + \theta^{\pm}_{1}\theta^{\pm}_{2}, \tag{8b}$$

$$2\eta^{\pm}_{\alpha 3} = \beta_{\alpha}\lambda^{\pm}_{\alpha} + \beta_{\gamma}\omega^{\pm}_{\alpha} - \beta_3\theta^{\pm}_{\alpha} \quad \text{for } \gamma \neq \alpha, \qquad \eta_{33} = \tfrac{1}{2}(\beta_1^2 + \beta_2^2 + \beta_3^2),$$

where

$$\begin{aligned}
\lambda^{\pm}_{\alpha} &= \left(\frac{1}{A_{\alpha}}v^{\pm}_{\alpha}\right)_{,\alpha} + B_{\alpha\alpha}v^{\pm}_{\alpha} + B_{\alpha\beta}v^{\pm}_{\beta} + k_{\alpha}v^{\pm}_{3} \quad \text{for } \beta \neq \alpha,\\
\omega^{\pm}_{\alpha} &= \left(\frac{1}{A_{\alpha}}v^{\pm}_{\beta}\right)_{,\alpha} + B_{\alpha\alpha}v^{\pm}_{\beta} - B_{\alpha\beta}v^{\pm}_{\alpha} \quad \text{for } \beta \neq \alpha,\\
\theta^{\pm}_{\alpha} &= -\left(\frac{1}{A_{\alpha}}v^{\pm}_{3}\right)_{,\alpha} - B_{\alpha\alpha}v^{\pm}_{3} + k_{\alpha}v^{\pm}_{\alpha}, \quad \beta_i = \frac{1}{h}(v^{+}_{i} - v^{-}_{i}), \quad B_{\alpha\delta} = \frac{1}{A_{\alpha}A_{\delta}}A_{\alpha,\delta}.
\end{aligned} \tag{9}$$

It should be noted that derivatives from Eq. (9) have been written in a form that is best suited for applying the analytical integration.

4. FE formulation

In this section the basic theoretical and computational aspects of the assumed stress–strain TM shell formulation including the analytical integration yielding the element stiffness matrix and two approaches for solving incremental equilibrium equations are addressed in detail.

4.1. Mixed variational equation

The Hu–Washizu 3D variational principle for the thin multilayered anisotropic shell can be written in the following form:

$$\begin{aligned}
&\sum_{k}\int\int\int_{V_k}\sum_{i,j}\left[\left(S^{(k)}_{ij} - \sum_{\ell,m}C^{(k)}_{ij\ell m}\varepsilon^{AS}_{\ell m}\right)\delta\varepsilon^{AS}_{ij} + (\varepsilon^{AS}_{ij} - \varepsilon^{DS}_{ij})\delta S^{(k)}_{ij} - S^{(k)}_{ij}\delta\varepsilon^{DS}_{ij}\right]\mathrm{d}\alpha_3\,\mathrm{d}S\\
&\quad + \int\int_{S^+}\sum_{i}p^{+}_{i}\,\delta u_i\,\mathrm{d}S - \int\int_{S^-}\sum_{i}p^{-}_{i}\,\delta u_i\,\mathrm{d}S\\
&\quad + \sum_{k}\int\int_{\Omega_k}(q^{(k)}_{\nu}\,\delta u_{\nu} + q^{(k)}_{t}\,\delta u_t + q^{(k)}_{3}\,\delta u_3)\mathrm{d}\Omega = 0,
\end{aligned} \tag{10a}$$

$$\mathrm{d}S = \overline{A}_1\overline{A}_2\,\mathrm{d}\alpha_1\,\mathrm{d}\alpha_2, \quad \mathrm{d}\Omega = \bar{\gamma}\,\mathrm{d}\alpha_3\,\mathrm{d}s, \tag{10b}$$

$$\overline{A}_{\alpha} = A_{\alpha}(1 + k_{\alpha}\bar{\delta}), \quad \bar{\gamma} = 1 + k_N\bar{\delta}, \quad \bar{\delta} = \tfrac{1}{2}(\delta^{-} + \delta^{+}),$$

where $S^{(k)}_{ij}$ are the components of the second Piola–Kirchhoff stress tensor of the kth layer; $C^{(k)}_{ij\ell m}$ are the components of the elasticity tensor of the kth layer; ε^{DS}_{ij} are the strains due to the displacement field; ε^{AS}_{ij} are the independently assumed strains; u_{ν}, u_t and u_3 are the components of the displacement vector in the coordinate system ν, t and α_3 (see Fig. 1); k_N is the normal curvature of the bounding curve Γ. Here, in accordance with formulas (10b) it is supposed that the metrics of all surfaces parallel to the reference surface are *identical* and equal to the metric of the middle surface.

The finite deformation TM shell theory is based on the linear approximations of displacements (1) and displacement-dependent strains (2) in the thickness direction. Additionally, we should adopt the similar approximation for the assumed displacement-independent strains

$$\varepsilon^{AS}_{\alpha\beta} = N^-(\alpha_3)E^-_{\alpha\beta} + N^+(\alpha_3)E^+_{\alpha\beta}, \tag{11a}$$

$$\varepsilon^{AS}_{\alpha 3} = N^-(\alpha_3)E^-_{\alpha 3} + N^+(\alpha_3)E^+_{\alpha 3}, \tag{11b}$$

$$\varepsilon^{AS}_{33} = E_{33}. \tag{11c}$$

Substituting approximations (1), (2) and (11) into variational equation (10a) and introducing stress resultants and external load resultants

$$H^{\pm}_{\alpha i} = \sum_k \int_{\delta_{k-1}}^{\delta_k} S^{(k)}_{\alpha i} N^{\pm}(\alpha_3)\,\mathrm{d}\alpha_3, \quad H_{33} = \sum_k \int_{\delta_{k-1}}^{\delta_k} S^{(k)}_{33}\,\mathrm{d}\alpha_3,$$

$$\widehat{H}^{\pm}_{\nu\text{æ}} = \sum_k \int_{\delta_{k-1}}^{\delta_k} q^{(k)}_{\text{æ}} N^{\pm}(\alpha_3)\,\mathrm{d}\alpha_3 \qquad (\text{æ} = \nu, t, 3), \tag{12}$$

one can obtain the mixed variational equation for the TM shell element

$$\int_{-1}^{1}\int_{-1}^{1} [\delta\mathbf{E}^{\mathrm{T}}(\mathbf{H} - \mathbf{D}\mathbf{E}) + \delta\mathbf{H}^{\mathrm{T}}(\mathbf{E} - \boldsymbol{\mathscr{E}}) - \delta\boldsymbol{\mathscr{E}}^{\mathrm{T}}\mathbf{H} + \delta\mathbf{v}^{\mathrm{T}}\mathbf{P}]\overline{A}^{e\ell}_1\overline{A}^{e\ell}_2\,\mathrm{d}\xi_1\,\mathrm{d}\xi_2 + \oint_{\Gamma^{e\ell}} \delta\mathbf{v}^{\mathrm{T}}_{\Gamma}\widehat{\mathbf{H}}_{\Gamma}\bar{\gamma}\,\mathrm{d}s = 0. \tag{13}$$

Here, matrix notations are used

$$\mathbf{v} = [\,v^-_1 \quad v^+_1 \quad v^-_2 \quad v^+_2 \quad v^-_3 \quad v^+_3\,]^{\mathrm{T}}, \quad \mathbf{v}_{\Gamma} = [\,v^-_{\nu} \quad v^+_{\nu} \quad v^-_t \quad v^+_t \quad v^-_3 \quad v^+_3\,]^{\mathrm{T}},$$

$$\boldsymbol{\mathscr{E}} = \left[\,\mathscr{E}^-_{11} \quad \mathscr{E}^+_{11} \quad \mathscr{E}^-_{22} \quad \mathscr{E}^+_{22} \quad 2\mathscr{E}^-_{12} \quad 2\mathscr{E}^+_{12} \quad 2\mathscr{E}^-_{13} \quad 2\mathscr{E}^+_{13} \quad 2\mathscr{E}^-_{23} \quad 2\mathscr{E}^+_{23} \quad \mathscr{E}_{33}\,\right]^{\mathrm{T}},$$

$$\mathbf{E} = \left[\,E^-_{11} \quad E^+_{11} \quad E^-_{22} \quad E^+_{22} \quad 2E^-_{12} \quad 2E^+_{12} \quad 2E^-_{13} \quad 2E^+_{13} \quad 2E^-_{23} \quad 2E^+_{23} \quad E_{33}\,\right]^{\mathrm{T}},$$

$$\mathbf{H} = [\,H^-_{11} \quad H^+_{11} \quad H^-_{22} \quad H^+_{22} \quad H^-_{12} \quad H^+_{12} \quad H^-_{13} \quad H^+_{13} \quad H^-_{23} \quad H^+_{23} \quad H_{33}\,]^{\mathrm{T}},$$

$$\widehat{\mathbf{H}}_{\Gamma} = [\,\widehat{H}^-_{\nu\nu} \quad \widehat{H}^+_{\nu\nu} \quad \widehat{H}^-_{\nu t} \quad \widehat{H}^+_{\nu t} \quad \widehat{H}^-_{\nu 3} \quad \widehat{H}^+_{\nu 3}\,]^{\mathrm{T}}, \quad \mathbf{P} = [\,-p^-_1 \quad p^+_1 \quad -p^-_2 \quad p^+_2 \quad -p^-_3 \quad p^+_3\,]^{\mathrm{T}},$$

$$\mathbf{D} = \begin{bmatrix}
D^{00}_{1111} & D^{01}_{1111} & D^{00}_{1122} & D^{01}_{1122} & D^{00}_{1112} & D^{01}_{1112} & 0 & 0 & 0 & 0 & D^-_{1133} \\
D^{01}_{1111} & D^{11}_{1111} & D^{01}_{1122} & D^{11}_{1122} & D^{01}_{1112} & D^{11}_{1112} & 0 & 0 & 0 & 0 & D^+_{1133} \\
D^{00}_{2211} & D^{01}_{2211} & D^{00}_{2222} & D^{01}_{2222} & D^{00}_{2212} & D^{01}_{2212} & 0 & 0 & 0 & 0 & D^-_{2233} \\
D^{01}_{2211} & D^{11}_{2211} & D^{01}_{2222} & D^{11}_{2222} & D^{01}_{2212} & D^{11}_{2212} & 0 & 0 & 0 & 0 & D^+_{2233} \\
D^{00}_{1211} & D^{01}_{1211} & D^{00}_{1222} & D^{01}_{1222} & D^{00}_{1212} & D^{01}_{1212} & 0 & 0 & 0 & 0 & D^-_{1233} \\
D^{01}_{1211} & D^{11}_{1211} & D^{01}_{1222} & D^{11}_{1222} & D^{01}_{1212} & D^{11}_{1212} & 0 & 0 & 0 & 0 & D^+_{1233} \\
0 & 0 & 0 & 0 & 0 & 0 & D^{00}_{1313} & D^{01}_{1313} & D^{00}_{1323} & D^{01}_{1323} & 0 \\
0 & 0 & 0 & 0 & 0 & 0 & D^{01}_{1313} & D^{11}_{1313} & D^{01}_{1323} & D^{11}_{1323} & 0 \\
0 & 0 & 0 & 0 & 0 & 0 & D^{00}_{2313} & D^{01}_{2313} & D^{00}_{2323} & D^{01}_{2323} & 0 \\
0 & 0 & 0 & 0 & 0 & 0 & D^{01}_{2313} & D^{11}_{2313} & D^{01}_{2323} & D^{11}_{2323} & 0 \\
D^-_{3311} & D^+_{3311} & D^-_{3322} & D^+_{3322} & D^-_{3312} & D^+_{3312} & 0 & 0 & 0 & 0 & D_{3333}
\end{bmatrix}, \tag{14}$$

$$D^{pq}_{ij\ell m} = \sum_k \int_{\delta_{k-1}}^{\delta_k} C^{(k)}_{ij\ell m}[N^-(\alpha_3)]^{2-p-q}[N^+(\alpha_3)]^{p+q}\,\mathrm{d}\alpha_3 \quad \text{for } p, q = 0, 1,$$

$$D^-_{33\ell m} = D^{00}_{33\ell m} + D^{01}_{33\ell m}, \quad D^+_{33\ell m} = D^{01}_{33\ell m} + D^{11}_{33\ell m}, \quad D_{3333} = D^-_{3333} + D^+_{3333},$$

where $\xi_\gamma = (\alpha_\gamma - d^{e\ell}_\gamma)/\ell^{e\ell}_\gamma$ are the local curvilinear normalized coordinates (see Fig. 3); $d^{e\ell}_\gamma = (\alpha^{-e\ell}_\gamma + \alpha^{+e\ell}_\gamma)/2$ are the coordinates of the center of the element; $2\ell^{e\ell}_\gamma = \alpha^{+e\ell}_\gamma - \alpha^{-e\ell}_\gamma$ are the lengths of the element; $\overline{A}^{e\ell}_\alpha = \overline{A}_\alpha \ell^{e\ell}_\alpha$ are the Lamé coefficients of the middle surface of the element; $v^{\pm}_\nu$, $v^{\pm}_t$ and $v^{\pm}_3$ are the components of the

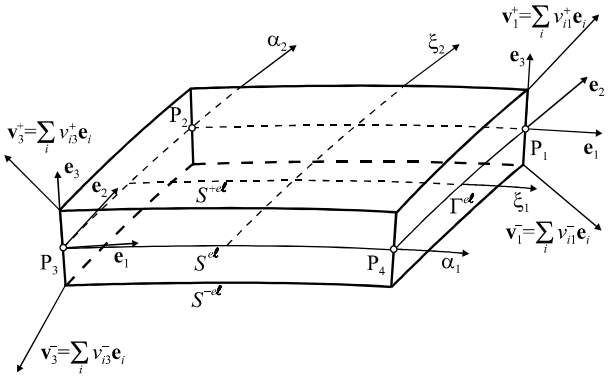

Fig. 3. Four-node curved shell element. $P_1(\alpha_1^{+e\ell},\alpha_2^{+e\ell}), P_2(\alpha_1^{-e\ell},\alpha_2^{+e\ell}), P_3(\alpha_1^{-e\ell},\alpha_2^{-e\ell}), P_4(\alpha_1^{+e\ell},\alpha_2^{-e\ell})$ are the nodal points of the element.

displacement vectors of the face surfaces in the coordinate system ν, t and α_3; $D_{ij\ell m}^{pq}$ are the components of the through-the-thickness elasticity tensors; $\Gamma^{e\ell}$ is the bounding curve belonging to the reference surface of the element $S^{e\ell}$.

Variational equation (13) provides a foundation for the FE formulation on the basis of two approaches for circumventing thickness locking with the non-symmetric constitutive stiffness matrix **D** [3,16] when $D_{\alpha\beta 33}^{\pm}=0$ or symmetric one [11–14] when additionally $D_{33\alpha\beta}^{\pm}=0$. Below only the first approach will be employed.

4.2. Four-node curved TM shell element

For the simplest quadrilateral four-node shell element the displacement field is approximated according to the standard C^0 interpolation

$$\mathbf{v}=\sum_r N_r(\xi_1,\xi_2)\mathbf{v}_r \quad \text{or} \tag{15a}$$

$$\mathbf{v}=\sum_{r_1,r_2}\xi_1^{r_1}\xi_2^{r_2}\mathbf{v}^{r_1r_2}, \tag{15b}$$

where $\mathbf{v}_r=[\,v_{1r}^-\quad v_{1r}^+\quad v_{2r}^-\quad v_{2r}^+\quad v_{3r}^-\quad v_{3r}^+\,]^{\mathrm{T}}$ are the displacement vectors of the element nodes; $N_r(\xi_1,\xi_2)$ are the linear shape functions of the element; the subscript r denotes a number of nodes and runs from 1 to 4; superscripts r_1, r_2 take the values 0 and 1. The load vector is also assumed to vary linearly inside the element.

In a result for the displacement-dependent strains (7) and (8) we have the following approximation:

$$\boldsymbol{\mathscr{E}}=\sum_{s_1,s_2}\xi_1^{s_1}\xi_2^{s_2}\boldsymbol{\mathscr{E}}^{s_1s_2}, \tag{16a}$$

$$\boldsymbol{\mathscr{E}}^{s_1s_2}=(\mathbf{B}^{s_1s_2}+\mathbf{A}^{s_1s_2}\mathbf{V})\mathbf{V},\quad \mathbf{B}^{s_1s_2}=\mathbf{0}\qquad \text{for } s_1=2 \text{ or } s_2=2, \tag{16b}$$

$$\boldsymbol{\mathscr{E}}^{s_1s_2}=[\,\mathscr{E}_{11}^{-s_1s_2}\quad \mathscr{E}_{11}^{+s_1s_2}\quad \mathscr{E}_{22}^{-s_1s_2}\quad \mathscr{E}_{22}^{+s_1s_2}\quad 2\mathscr{E}_{12}^{-s_1s_2}\quad 2\mathscr{E}_{12}^{+s_1s_2}\quad 2\mathscr{E}_{13}^{-s_1s_2}\quad 2\mathscr{E}_{13}^{+s_1s_2}\quad 2\mathscr{E}_{23}^{-s_1s_2}\quad 2\mathscr{E}_{23}^{+s_1s_2}\quad \mathscr{E}_{33}^{s_1s_2}\,]^{\mathrm{T}},$$

where $\mathbf{V}=[\,\mathbf{v}_1^{\mathrm{T}}\quad \mathbf{v}_2^{\mathrm{T}}\quad \mathbf{v}_3^{\mathrm{T}}\quad \mathbf{v}_4^{\mathrm{T}}\,]^{\mathrm{T}}$ is the displacement vector at nodal points of the element; $\mathbf{B}^{s_1s_2}$ are the matrices of order 11×24 corresponding to the linear strain–displacement transformation; $\mathbf{A}^{s_1s_2}$ are the 3D arrays of order $11\times 24\times 24$ corresponding to the non-linear strain–displacement transformation. Throughout this section superscripts s_1, s_2 take the values 0, 1 and 2.

Remark 1. The higher-order coefficients in approximation (16a) and (16b) for the transverse shear strains satisfy the following coupling conditions:

$$\mathscr{E}_{13}^{-2s_2} = \mathscr{E}_{13}^{+2s_2} \quad \text{and} \quad \mathscr{E}_{23}^{-s_1 2} = \mathscr{E}_{23}^{+s_1 2}, \tag{16c}$$

which follow from strain–displacement relationships (7)–(9) and have a common nature with kinematic conditions (4).

To avoid shear and membrane locking and have no spurious zero energy modes, the assumed strain and stress resultant fields inside the element are introduced

$$\begin{aligned}
&\mathbf{E} = \sum_{r_1,r_2} \xi_1^{r_1} \xi_2^{r_2} \mathbf{Q}^{r_1 r_2} \mathbf{E}^{r_1 r_2}, \quad \mathbf{H} = \sum_{r_1,r_2} \xi_1^{r_1} \xi_2^{r_2} \mathbf{Q}^{r_1 r_2} \mathbf{H}^{r_1 r_2},\\
&\mathbf{E}^{00} = [\,E_{11}^{-00} \quad E_{11}^{+00} \quad E_{22}^{-00} \quad E_{22}^{+00} \quad 2E_{12}^{-00} \quad 2E_{12}^{+00} \quad 2E_{13}^{-00} \quad 2E_{13}^{+00} \quad 2E_{23}^{-00} \quad 2E_{23}^{+00} \quad E_{33}^{00}\,]^{\mathrm{T}},\\
&\mathbf{E}^{01} = [\,E_{11}^{-01} \quad E_{11}^{+01} \quad 2E_{13}^{-01} \quad 2E_{13}^{+01} \quad E_{33}^{01}\,]^{\mathrm{T}},\\
&\mathbf{E}^{10} = [\,E_{22}^{-10} \quad E_{22}^{+10} \quad 2E_{23}^{-10} \quad 2E_{23}^{+10} \quad E_{33}^{10}\,]^{\mathrm{T}},\\
&\mathbf{E}^{11} = [E_{33}^{11}],\\
&\mathbf{H}^{00} = [\,H_{11}^{-00} \quad H_{11}^{+00} \quad H_{22}^{-00} \quad H_{22}^{+00} \quad H_{12}^{-00} \quad H_{12}^{+00} \quad H_{13}^{-00} \quad H_{13}^{+00} \quad H_{23}^{-00} \quad H_{23}^{+00} \quad H_{33}^{00}\,]^{\mathrm{T}},\\
&\mathbf{H}^{01} = [\,H_{11}^{-01} \quad H_{11}^{+01} \quad H_{13}^{-01} \quad H_{13}^{+01} \quad H_{33}^{01}\,]^{\mathrm{T}},\\
&\mathbf{H}^{10} = [\,H_{22}^{-10} \quad H_{22}^{+10} \quad H_{23}^{-10} \quad H_{23}^{+10} \quad H_{33}^{10}\,]^{\mathrm{T}},\\
&\mathbf{H}^{11} = [H_{33}^{11}],
\end{aligned} \tag{17}$$

where $\mathbf{Q}^{r_1 r_2}$ are the matrices from zeros and units defined in Part I [3]. Note that this approach may be treated as an assumed stress–strain formulation and was proposed by Wempner et al. [10] for the geometrically linear TM shells without the thickness change. Further developments for the geometrically non-linear Timoshenko beam, Mindlin plate and TM shell theories can be found in Refs. [1–3].

It is important that the described formulation makes our non-linear four-node curved TM shell element a bit stiff. The best solution of the problem is to use the assumed displacement-dependent strain field [1]. The main idea of the such formulation may be traced back to the ANS method proposed by Hughes and Tezduyar [21] for the linear displacement FE formulation and further developed by many scientists for the non-linear displacement and mixed FE formulations [4–7,22–24]. This enhanced non-linear FE formulation has been already used in Part I [3], but has not been described for conciseness.

To circumvent *non-linear locking*, displacement-dependent strains are assumed to vary linearly inside the element (see Fig. 3)

$$\boldsymbol{\mathscr{E}}^{ADS} = \sum_r N_r(\xi_1, \xi_2) \boldsymbol{\mathscr{E}}(P_r) \tag{18}$$

that may be written by using Eq. (16a) in the more convenient form

$$\boldsymbol{\mathscr{E}}^{ADS} = \boldsymbol{\mathscr{E}}^{00} + \boldsymbol{\mathscr{E}}^{02} + \boldsymbol{\mathscr{E}}^{20} + \boldsymbol{\mathscr{E}}^{22} + \xi_1(\boldsymbol{\mathscr{E}}^{10} + \boldsymbol{\mathscr{E}}^{12}) + \xi_2(\boldsymbol{\mathscr{E}}^{01} + \boldsymbol{\mathscr{E}}^{21}) + \xi_1\xi_2\boldsymbol{\mathscr{E}}^{11}. \tag{19}$$

Substituting Eqs. (15b), (17) and (19) into mixed variational equation (13) and using the standard variational procedure, one obtains governing equations of the developed FE formulation

$$\mathbf{E}^{r_1 r_2} = (\mathbf{Q}^{r_1 r_2})^{\mathrm{T}} (\mathbf{B}^{r_1 r_2} + \mathbf{R}^{r_1 r_2} \mathbf{V}) \mathbf{V}, \tag{20a}$$

$$\mathbf{H}^{r_1 r_2} = (\mathbf{Q}^{r_1 r_2})^{\mathrm{T}} \mathbf{D} \mathbf{Q}^{r_1 r_2} \mathbf{E}^{r_1 r_2}, \tag{20b}$$

$$\sum_{r_1,r_2} \frac{1}{3^{r_1+r_2}} (\mathbf{B}^{r_1 r_2} + 2\mathbf{R}^{r_1 r_2} \mathbf{V})^{\mathrm{T}} \mathbf{Q}^{r_1 r_2} \mathbf{H}^{r_1 r_2} = \mathbf{F}, \tag{20c}$$

where $\mathbf{F}$ is the force vector; $\mathbf{R}^{r_1r_2}$ are the 3D arrays of order $11\times 24\times 24$ defined as

$$\mathbf{R}^{00}=\mathbf{A}^{00}+\mathbf{A}^{02}+\mathbf{A}^{20}+\mathbf{A}^{22},\quad \mathbf{R}^{01}=\mathbf{A}^{01}+\mathbf{A}^{21},\quad \mathbf{R}^{10}=\mathbf{A}^{10}+\mathbf{A}^{12},\quad \mathbf{R}^{11}=\mathbf{A}^{11}. \tag{21}$$

Remark 2. There exists a link between displacement-independent and displacement-dependent strains

$$\begin{aligned}&\mathbf{E}^{00}=\boldsymbol{\mathscr{E}}^{00}+\boldsymbol{\mathscr{E}}^{02}+\boldsymbol{\mathscr{E}}^{20}+\boldsymbol{\mathscr{E}}^{22},\\ &\mathbf{E}^{01}=(\mathbf{Q}^{01})^{\mathrm{T}}(\boldsymbol{\mathscr{E}}^{01}+\boldsymbol{\mathscr{E}}^{21}),\quad \mathbf{E}^{10}=(\mathbf{Q}^{10})^{\mathrm{T}}(\boldsymbol{\mathscr{E}}^{10}+\boldsymbol{\mathscr{E}}^{12}),\quad \mathbf{E}^{11}=(\mathbf{Q}^{11})^{\mathrm{T}}\boldsymbol{\mathscr{E}}^{11}\end{aligned} \tag{22}$$

that immediately follows from Eq. (20a) allowing for Eqs. (16b) and (21).

4.3. Analytical integration leading to element stiffness matrix

In order to fulfill an analytical integration after substitution of the linear interpolations (15b), (17) and (19) into variational equation (13), we should invoke non-traditional schemes for evaluating strains of the face surfaces from Eqs. (7), (8) and (16b)

$$\mathscr{E}_{\alpha i}^{\pm s_1s_2}=e_{\alpha i}^{\pm s_1s_2}+\eta_{\alpha i}^{\pm s_1s_2},\quad \mathscr{E}_{33}^{s_1s_2}=e_{33}^{s_1s_2}+\eta_{33}^{s_1s_2}, \tag{23a}$$

$$e_{\alpha\alpha}^{\pm r_1r_2}=\{\zeta_\alpha^{\pm}\}^{00}\lambda_\alpha^{\pm r_1r_2},\quad 2e_{12}^{\pm r_1r_2}=\{\zeta_2^{\pm}\}^{00}\omega_1^{\pm r_1r_2}+\{\zeta_1^{\pm}\}^{00}\omega_2^{\pm r_1r_2}, \tag{23b}$$

$$\begin{aligned}&2e_{\alpha 3}^{\pm r_1r_2}=\{\zeta_\alpha^{\pm}\}^{00}\beta_\alpha^{r_1r_2}-\theta_\alpha^{\pm r_1r_2},\quad e_{33}^{r_1r_2}=\beta_3^{r_1r_2},\\ &e_{\alpha i}^{\pm s_1s_2}=0\quad\text{and}\quad e_{33}^{s_1s_2}=0\qquad\text{for } s_1=2 \text{ or } s_2=2,\end{aligned}$$

$$\eta_{\alpha\alpha}^{\pm s_1s_2}=\frac{1}{2}\sum_{\substack{r_1+r_3=s_1\\ r_2+r_4=s_2}}(\lambda_\alpha^{\pm r_1r_2}\lambda_\alpha^{\pm r_3r_4}+\omega_\alpha^{\pm r_1r_2}\omega_\alpha^{\pm r_3r_4}+\theta_\alpha^{\pm r_1r_2}\theta_\alpha^{\pm r_3r_4}), \tag{23c}$$

$$2\eta_{12}^{\pm s_1s_2}=\sum_{\substack{r_1+r_3=s_1\\ r_2+r_4=s_2}}(\lambda_1^{\pm r_1r_2}\omega_2^{\pm r_3r_4}+\lambda_2^{\pm r_1r_2}\omega_1^{\pm r_3r_4}+\theta_1^{\pm r_1r_2}\theta_2^{\pm r_3r_4}),$$

$$2\eta_{\alpha 3}^{\pm s_1s_2}=\sum_{\substack{r_1+r_3=s_1\\ r_2+r_4=s_2}}(\beta_\alpha^{r_1r_2}\lambda_\alpha^{\pm r_3r_4}+\beta_\gamma^{r_1r_2}\omega_\alpha^{\pm r_3r_4}-\beta_3^{r_1r_2}\theta_\alpha^{\pm r_3r_4})\quad(\gamma\neq\alpha),$$

$$\eta_{33}^{s_1s_2}=\frac{1}{2}\sum_{\substack{r_1+r_3=s_1\\ r_2+r_4=s_2}}(\beta_1^{r_1r_2}\beta_1^{r_3r_4}+\beta_2^{r_1r_2}\beta_2^{r_3r_4}+\beta_3^{r_1r_2}\beta_3^{r_3r_4}),$$

where

$$\begin{aligned}&\lambda_\alpha^{\pm r_1r_2}=\left\{\frac{1}{A_\alpha^{e\ell}}v_\alpha^{\pm}\right\}_\alpha^{r_1r_2}+\{B_{\alpha\alpha}^{e\ell}v_\alpha^{\pm}+B_{\alpha\beta}^{e\ell}v_\beta^{\pm}+k_\alpha v_3^{\pm}\}^{r_1r_2}\ (\beta\neq\alpha),\\ &\omega_\alpha^{\pm r_1r_2}=\left\{\frac{1}{A_\alpha^{e\ell}}v_\beta^{\pm}\right\}_\alpha^{r_1r_2}+\{B_{\alpha\alpha}^{e\ell}v_\beta^{\pm}-B_{\alpha\beta}^{e\ell}v_\alpha^{\pm}\}^{r_1r_2}\ (\beta\neq\alpha),\\ &\theta_\alpha^{\pm r_1r_2}=-\left\{\frac{1}{A_\alpha^{e\ell}}v_3^{\pm}\right\}_\alpha^{r_1r_2}+\{-B_{\alpha\alpha}^{e\ell}v_3^{\pm}+k_\alpha v_\alpha^{\pm}\}^{r_1r_2},\quad \beta_i^{r_1r_2}=\frac{1}{h}(v_i^{+r_1r_2}-v_i^{-r_1r_2}).\end{aligned} \tag{24}$$

In formulas (23) and (24) superscripts r_1, r_2, r_3 and r_4 take the values 0 and 1, while s_1 and s_2 run from 0 to 2, and in accordance with Fig. 3 convenient mesh notations are used

$$\begin{aligned}
&\{f\}^{00} = \tfrac{1}{4}[f(P_1)+f(P_2)+f(P_3)+f(P_4)], \quad \{f\}^{01} = \tfrac{1}{4}[f(P_1)+f(P_2)-f(P_3)-f(P_4)],\\
&\{f\}^{10} = \tfrac{1}{4}[f(P_1)-f(P_2)-f(P_3)+f(P_4)], \quad \{f\}^{11} = \tfrac{1}{4}[f(P_1)-f(P_2)+f(P_3)-f(P_4)],\\
&\{f\}_1^{00} = \{f\}^{10}, \quad \{f\}_1^{01} = \{f\}^{11}, \quad \{f\}_1^{10} = \{f\}_1^{11} = 0,\\
&\{f\}_2^{00} = \{f\}^{01}, \quad \{f\}_2^{10} = \{f\}^{11}, \quad \{f\}_2^{01} = \{f\}_2^{11} = 0.
\end{aligned} \tag{25}$$

Assuming further that a product $\overline{A}_1^{e\ell}\overline{A}_2^{e\ell}$ from the variational equation (13) does not vary inside the element and accounting for notations (25), the simplest approximation can be employed

$$\overline{A}_1^{e\ell}\overline{A}_2^{e\ell} = \{\overline{A}_1^{e\ell}\overline{A}_2^{e\ell}\}^{00}. \tag{26}$$

It is remarkable that our elemental stiffness matrix requires only direct substitutions (no inversion is needed as we shall see in the next section) and it is evaluated by using the analytical integration. So, our FE formulation is very economical and efficient compared to the conventional isoparametric FE formulations because it reduces the costly numerical integration by deriving the elemental stiffness matrices.

4.4. Two approaches for solving incremental equilibrium equations

Up to this moment, no incremental arguments are needed in the total Lagrangian formulation. The incremental displacements, strains and stress resultants are needed for solving non-linear equations (20) on the basis of the Newton–Raphson method. Further, the left superscripts t and $t+\Delta t$ indicate in which configuration at time t or time $t+\Delta t$ a quantity occurs. Then, in accordance with this agreement we have

$${}^{t+\Delta t}\mathbf{V} = {}^{t}\mathbf{V} + \Delta\mathbf{V}, \quad {}^{t+\Delta t}\mathbf{F} = {}^{t}\mathbf{F} + \Delta\mathbf{F}, \quad {}^{t+\Delta t}\mathbf{E}^{r_1r_2} = {}^{t}\mathbf{E}^{r_1r_2} + \Delta\mathbf{E}^{r_1r_2}, \quad {}^{t+\Delta t}\mathbf{H}^{r_1r_2} = {}^{t}\mathbf{H}^{r_1r_2} + \Delta\mathbf{H}^{r_1r_2}, \tag{27}$$

where $\Delta\mathbf{V}, \Delta\mathbf{F}, \Delta\mathbf{E}^{r_1r_2}$ and $\Delta\mathbf{H}^{r_1r_2}$ are the incremental variables.

Substituting formulas (27) in Eq. (20) and taking into account that the external loads and second Piola-Kirchhoff stresses constitute the self-equilibrated system in a configuration at time t, one can obtain the following incremental equations:

$$\Delta\mathbf{E}^{r_1r_2} = (\mathbf{Q}^{r_1r_2})^{\mathrm{T}}({}^{t}\mathbf{M}^{r_1r_2} + \mathbf{R}^{r_1r_2}\Delta\mathbf{V})\Delta\mathbf{V}, \tag{28a}$$

$$\Delta\mathbf{H}^{r_1r_2} = \overline{\mathbf{D}}^{r_1r_2}\Delta\mathbf{E}^{r_1r_2}, \tag{28b}$$

$$\sum_{r_1,r_2}\frac{1}{3^{r_1+r_2}}[2(\mathbf{R}^{r_1r_2}\Delta\mathbf{V})^{\mathrm{T}}\mathbf{Q}^{r_1r_2}{}^{t}\mathbf{H}^{r_1r_2} + ({}^{t}\mathbf{M}^{r_1r_2} + 2\mathbf{R}^{r_1r_2}\Delta\mathbf{V})^{\mathrm{T}}\mathbf{Q}^{r_1r_2}\Delta\mathbf{H}^{r_1r_2}] = \Delta\mathbf{F}. \tag{28c}$$

Here and in the following developments convenient matrix notations are used

$$\overline{\mathbf{D}}^{r_1r_2} = (\mathbf{Q}^{r_1r_2})^{\mathrm{T}}\mathbf{D}\mathbf{Q}^{r_1r_2}, \quad \mathbf{D}^{r_1r_2} = \mathbf{Q}^{r_1r_2}\overline{\mathbf{D}}^{r_1r_2}(\mathbf{Q}^{r_1r_2})^{\mathrm{T}}, \tag{29a}$$

$${}^{t}\mathbf{M}^{r_1r_2} = \mathbf{B}^{r_1r_2} + 2\mathbf{R}^{r_1r_2}{}^{t}\mathbf{V}. \tag{29b}$$

There are two approaches for solving incremental equations (28). The first approach developed in Part I [3] practically leads to the displacement FE formulation while the second approach yields the classical hybrid FE formulation [17–19].

4.4.1. Approach D

Let us eliminate incremental strains and stress resultants from Eq. (28). In a result, the following equilibrium equations are obtained

$$\sum_{r_1,r_2}\frac{1}{3^{r_1+r_2}}[2(\mathbf{R}^{r_1r_2}\Delta\mathbf{V})^{\mathrm{T}}\mathbf{Q}^{r_1r_2}{}^{t}\mathbf{H}^{r_1r_2} + ({}^{t}\mathbf{M}^{r_1r_2} + 2\mathbf{R}^{r_1r_2}\Delta\mathbf{V})^{\mathrm{T}}\mathbf{D}^{r_1r_2}({}^{t}\mathbf{M}^{r_1r_2} + \mathbf{R}^{r_1r_2}\Delta\mathbf{V})\Delta\mathbf{V}] = \Delta\mathbf{F}, \tag{30}$$

where $\mathbf{D}^{r_1r_2}$ are the matrices of order 11×11 defined by Eq. (29a).

Due to existence of non-linear terms in Eq. (30), the Newton–Raphson iteration process should be employed

$$\Delta\mathbf{V}^{[n+1]} = \Delta\mathbf{V}^{[n]} + \Delta\boldsymbol{\mathscr{V}}^{[n]} \quad (n = 0, 1, \ldots) \tag{31}$$

to solve these equations

$$\sum_{r_1,r_2} \frac{1}{3^{r_1+r_2}} \Big[({}^t\mathbf{L}^{r_1r_2[n]})^{\mathrm{T}} \mathbf{D}^{r_1r_2\,t}\mathbf{L}^{r_1r_2[n]} \Delta\boldsymbol{\mathscr{V}}^{[n]} + 2(\mathbf{R}^{r_1r_2}\Delta\boldsymbol{\mathscr{V}}^{[n]})^{\mathrm{T}} (\mathbf{Q}^{r_1r_2\,t}\mathbf{H}^{r_1r_2} + \underline{\mathbf{D}^{r_1r_2}({}^t\mathbf{M}^{r_1r_2} + \mathbf{R}^{r_1r_2}\Delta\mathbf{V}^{[n]})\Delta\mathbf{V}^{[n]}}) \Big] = \Delta\mathscr{F}^{[n]}, \tag{32}$$

where

$$\Delta\mathscr{F}^{[n]} = \Delta\mathbf{F} - \sum_{r_1,r_2} \frac{1}{3^{r_1+r_2}} [2(\mathbf{R}^{r_1r_2}\Delta\mathbf{V}^{[n]})^{\mathrm{T}} \mathbf{Q}^{r_1r_2\,t}\mathbf{H}^{r_1r_2} + ({}^t\mathbf{L}^{r_1r_2[n]})^{\mathrm{T}} \mathbf{D}^{r_1r_2} ({}^t\mathbf{M}^{r_1r_2} + \mathbf{R}^{r_1r_2}\Delta\mathbf{V}^{[n]})\Delta\mathbf{V}^{[n]}],$$
$${}^t\mathbf{L}^{r_1r_2[n]} = \mathbf{B}^{r_1r_2} + 2\mathbf{R}^{r_1r_2}({}^t\mathbf{V} + \Delta\mathbf{V}^{[n]}). \tag{33}$$

The equilibrium equations (32) and (33) for each element are assembled by the usual technique to form the global incremental equilibrium equations. These incremental equations should be performed until the required accuracy of the solution can be obtained. The convergence criterion used herein can be described as

$$\|\Delta\mathbf{U}^{[n+1]} - \Delta\mathbf{U}^{[n]}\| < \varepsilon\|\Delta\mathbf{U}^{[n]}\|, \tag{34}$$

where $\|\cdot\|$ stands for the Euclidean norm in the displacement space; $\Delta\mathbf{U}$ is the global vector of displacement increments; ε is the prescribed tolerance.

4.4.2. Approach H

Here, it is discussed an alternative approach when equilibrium equations (28) for incremental displacements and incremental assumed strains and stress resultants are solved by the Newton–Raphson method simultaneously, i.e., a new iteration scheme should be applied

$$\Delta\mathbf{V}^{[n+1]} = \Delta\mathbf{V}^{[n]} + \Delta\boldsymbol{\mathscr{V}}^{[n]}, \quad \Delta\mathbf{E}^{r_1r_2[n+1]} = \Delta\mathbf{E}^{r_1r_2[n]} + \Delta\mathbf{E}^{r_1r_2[n]},$$
$$\Delta\mathbf{H}^{r_1r_2[n+1]} = \Delta\mathbf{H}^{r_1r_2[n]} + \Delta\mathscr{H}^{r_1r_2[n]} \quad (n = 0, 1, \ldots) \tag{35}$$

instead of scheme (31). As a result, we have

$$\Delta\mathbf{E}^{r_1r_2[n]} - (\mathbf{Q}^{r_1r_2})^{\mathrm{T}}\,{}^t\mathbf{L}^{r_1r_2[n]}\Delta\boldsymbol{\mathscr{V}}^{[n]} = (\mathbf{Q}^{r_1r_2})^{\mathrm{T}}({}^t\mathbf{M}^{r_1r_2} + \mathbf{R}^{r_1r_2}\Delta\mathbf{V}^{[n]})\Delta\mathbf{V}^{[n]} - \Delta\mathbf{E}^{r_1r_2[n]}, \tag{36a}$$

$$\Delta\mathscr{H}^{r_1r_2[n]} - \overline{\mathbf{D}}^{r_1r_2}\Delta\mathbf{E}^{r_1r_2[n]} = \overline{\mathbf{D}}^{r_1r_2}\Delta\mathbf{E}^{r_1r_2[n]} - \Delta\mathbf{H}^{r_1r_2[n]}, \tag{36b}$$

$$\sum_{r_1,r_2} \frac{1}{3^{r_1+r_2}} [2(\mathbf{R}^{r_1r_2}\Delta\boldsymbol{\mathscr{V}}^{[n]})^{\mathrm{T}} \mathbf{Q}^{r_1r_2}({}^t\mathbf{H}^{r_1r_2} + \Delta\mathbf{H}^{r_1r_2[n]}) + ({}^t\mathbf{L}^{r_1r_2[n]})^{\mathrm{T}} \mathbf{Q}^{r_1r_2}\Delta\mathscr{H}^{r_1r_2[n]}$$
$$= \Delta\mathbf{F} - \sum_{r_1,r_2} \frac{1}{3^{r_1+r_2}} [2(\mathbf{R}^{r_1r_2}\Delta\mathbf{V}^{[n]})^{\mathrm{T}} \mathbf{Q}^{r_1r_2\,t}\mathbf{H}^{r_1r_2} + ({}^t\mathbf{L}^{r_1r_2[n]})^{\mathrm{T}} \mathbf{Q}^{r_1r_2}\Delta\mathbf{H}^{r_1r_2[n]}]. \tag{36c}$$

Eliminating further incremental strains $\Delta\mathbf{E}^{r_1r_2[n]}$ and stress resultants $\Delta\mathscr{H}^{r_1r_2[n]}$ from Eq. (36), one derives the following governing equations:

$$\sum_{r_1,r_2} \frac{1}{3^{r_1+r_2}} [({}^t\mathbf{L}^{r_1r_2[n]})^{\mathrm{T}} \mathbf{D}^{r_1r_2\,t}\mathbf{L}^{r_1r_2[n]}\Delta\boldsymbol{\mathscr{V}}^{[n]} + 2(\mathbf{R}^{r_1r_2}\Delta\boldsymbol{\mathscr{V}}^{[n]})^{\mathrm{T}} \mathbf{Q}^{r_1r_2}({}^t\mathbf{H}^{r_1r_2} + \underline{\Delta\mathbf{H}^{r_1r_2[n]}})] = \Delta\mathscr{F}^{[n]}. \tag{37}$$

It is observed that governing Eqs. (32) and (37) have equal right parts (33) and only underlined terms are different. These equations would be identical if an equality

$$\mathbf{Q}^{r_1r_2}\Delta\mathbf{H}^{r_1r_2[n]} = \mathbf{D}^{r_1r_2}({}^t\mathbf{M}^{r_1r_2} + \mathbf{R}^{r_1r_2}\Delta\mathbf{V}^{[n]})\Delta\mathbf{V}^{[n]} \tag{38}$$

would be fulfilled. This implies that compatibility conditions (28a) and (28b) are satisfied at every iteration step and, therefore, Approach H actually leads to Approach D. One can see that in Approach H the terms due to so-called compatibility mismatch [7,12,19] are present at every iteration step and disappear at the end of the iteration process.

Finally, we give a formula that is used in the numerical algorithm for the computation of incremental stress resultants at the nth iteration step

$$\mathbf{Q}^{r_1r_2}\Delta\mathbf{H}^{r_1r_2[n]} = \mathbf{D}^{r_1r_2}[({}^t\mathbf{M}^{r_1r_2} + 2\mathbf{R}^{r_1r_2}\Delta\mathbf{V}^{[n-1]})\Delta\mathbf{V}^{[n]} - (\mathbf{R}^{r_1r_2}\Delta\mathbf{V}^{[n-1]})\Delta\mathbf{V}^{[n-1]}] \tag{39}$$

instead of Eq. (38). This formula holds for $n \geqslant 1$ while at the beginning of the first iteration one should set

$$\Delta\mathbf{V}^{[0]} = \mathbf{0}, \quad \Delta\mathbf{H}^{r_1r_2[0]} = \mathbf{0}.$$

5. Numerical examples

The performance of the proposed TM shell elements is evaluated with several discriminating problems extracted from the literature. A listing of these elements and the abbreviations used to identify them are contained in Table 1.

In all numerical benchmark problems the tolerance error from criterion (34) is set to be $\varepsilon = 10^{-4}$. All our results are compared with those based on using identical node spacing and as a rule the same convergence tolerance. Besides, NStep denotes a number of load steps employed to equally divide the maximum load, whereas NIter stands for a number of iterations.

The computations were performed on a standard PC Pentium/1000 using Delphi environment. Note also that predictions of all elements developed (if they converge) are usually insensitive to a number of loading steps.

5.1. Examples demonstrating advantages of Approach H

The numerous benchmark problems exhibited that Approach H allows as a rule to use much larger load increments in comparison with Approach D and, therefore, H-elements are more efficient for engineering computations than D-elements. Some of these discriminating problems are a cantilever beam under the tip load, a pinched hemispherical shell, a slit ring plate, a cylindrical shell with free edges and a pinched cross-ply hyperbolic shell.

Table 1
Listing of elements

Name	Description
TMS4RD	Four-node curved TM shell element based on the Approach D [3]
TMS4RH	Four-node curved TM shell element based on the Approach H
HS (TL)	Bilinear hybrid stress solid-shell element based on the total Lagrangian formulation [7]
HS (UL)	Bilinear hybrid stress solid-shell element based on the updated Lagrangian formulation [7]
AS	Biquadratic assumed strain solid-shell element based on the total Lagrangian formulation [12]

5.1.1. Cantilever beam under transverse tip load

This problem has been extensively treated for numerical testing of non-linear FE models [7,12]. The cantilever beam has a rectangular cross-section, and its mechanical and geometrical characteristics are given in Fig. 4.

Table 2 lists a comparison with the results reported in Refs. [7,12] by using 8×1 and 4×1 regular meshes of bilinear and biquadratic solid-shell elements, respectively, with the numerical Gauss integration scheme. While we used the 8×1 mesh of TMS4R elements with an exact analytical integration. It is seen that both TMS4R elements yield an identical prediction of the beam response but the TMS4RH element solution converges more readily than the TMS4RD one. Fig. 5 additionally illustrates the dependence of tip displacements of the centerline on the loading factor f.

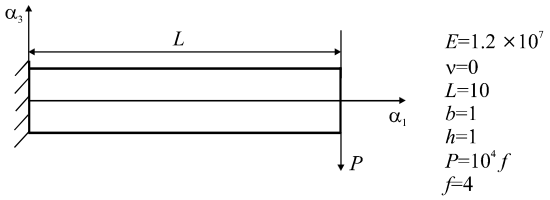

Fig. 4. Cantilever beam under transverse tip load.

Table 2
Tip displacements of cantilever beam under transverse load

Element	NStep = 1			NStep = 4			NStep = 10		
	$-\bar{v}_1$	$-\bar{v}_3$	NIter	$-\bar{v}_1$	$-\bar{v}_3$	NIter	$-\bar{v}_1$	$-\bar{v}_3$	NIter
TMS4RD	3.404	6.808	8	3.404	6.808	22	3.404	6.808	40
TMS4RH	3.404	6.808	5	3.404	6.808	12	3.404	6.808	29
HS (TL) [7]	3.344	6.777	5	3.344	6.777	14	3.344	6.777	30
HS (UL) [7]	3.357	6.785	7	3.357	6.785	17	3.357	6.785	36
AS [12]		6.766	6		6.761	16		6.761	34

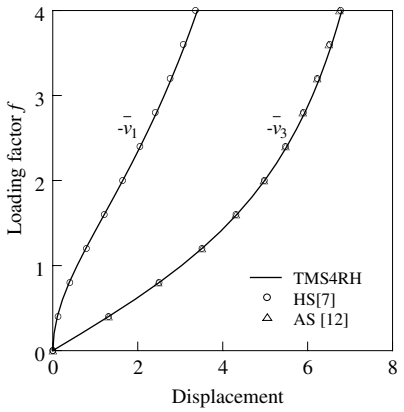

Fig. 5. Tip displacements of cantilever beam under transverse load.

5.1.2. Pinched hemispherical shell

To investigate the capability of the developed elements to overcome membrane and shear locking phenomena, we consider one of the most demanding non-linear tests. A hemispherical shell with 18° hole at the top is loaded by two pairs of opposite concentrated forces on the equator. The geometrical and material data of the problem are shown in Fig. 6.

Due to symmetry of the problem, only one quarter of the shell is modeled with 16×16 mesh of the TMS4R elements. Table 3 and Fig. 7 present a comparison with solutions [7,12] derived by using 16×16 and 8×8 uniform meshes of bilinear and biquadratic solid-shell elements, correspondingly. As can be seen, both TMS4R elements perform well but the TMS4RH element exhibits much better convergence characteristics. So, only seven iterations are needed to obtain a solution of this discriminating

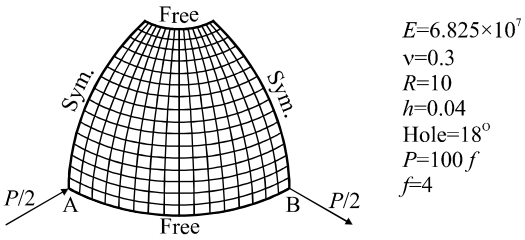

Fig. 6. Pinched hemispherical shell. Shell of revolution with geometrical parameters: $A_1 = R$, $A_2 = R\cos\alpha_1$, $k_1 = k_2 = 1/R$, $\alpha_1 \in [0, 2\pi/5]$, $\alpha_2 \in [0, \pi/2]$.

Table 3
Transverse displacements under applied loads of pinched hemispherical shell

Element	NStep = 1			NStep = 5			NStep = 10		
	$\bar{v}_3^B$	$-\bar{v}_3^A$	NIter	$\bar{v}_3^B$	$-\bar{v}_3^A$	NIter	$\bar{v}_3^B$	$-\bar{v}_3^A$	NIter
TMS4RD	Fail to converge			4.0556	8.1448	64	4.0556	8.1448	73
TMS4RH	4.0556	8.1448	7	4.0556	8.1448	17	4.0556	8.1448	29
HS (TL) [7]	4.0488	8.1173	8	4.0488	8.1173	21	4.0488	8.1173	36
HS (UL) [7]	4.0700	8.1783	10	4.0700	8.1784	26	4.0700	8.1784	44
AS [12]	4.0205	8.0160	8	4.0209	8.0169	23	4.0209	8.0169	35

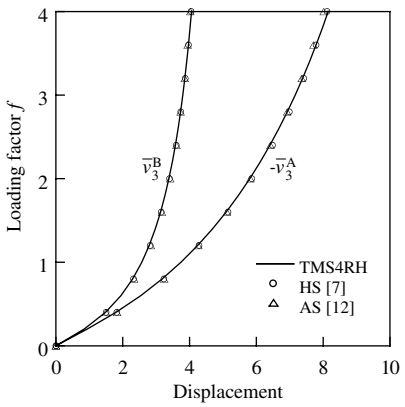

Fig. 7. Transverse displacements of pinched hemispherical shell.

problem. Note also that here, in contrast to Part I [3], the more robust strain–displacement relationships (7) and (8) were employed and, in a result, slightly more displacements were found.

5.1.3. Slit ring plate under line load

This example was first presented by Basar and Ding [25] to test finite deformation formulations for shell structures and further has been used by many investigators. The ring plate is subjected to a line load P applied at its free edge of the slit while the other edge is fully clamped. The plate is modeled by a shell of revolution with geometrical parameters shown in Fig. 8.

The displacements at points A and B of the plate, presented in Table 4 and Fig. 9, have been obtained using the 6×30 mesh of TMS4R elements and are compared with those reported in Refs. [7,26] by applying

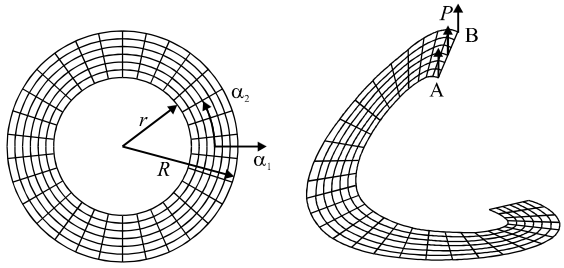

Fig. 8. Slit ring plate under line load. $E = 2.1 \times 10^7$, $v = 0$, $r = 6$, $R = 10$, $h = 0.03$, $P = 0.8$. Shell of revolution with geometrical parameters: $A_1 = 1$, $A_2 = r + \alpha_1$, $k_1 = 0$, $k_2 = 0$, $\alpha_1 \in [0, R - r]$, $\alpha_2 \in [0, 2\pi]$.

Table 4
Displacements at points A and B of slit ring plate

Element	NStep = 1			NStep = 5			NStep = 10		
	$\bar{v}_3^A$	$\bar{v}_3^B$	NIter	$\bar{v}_3^A$	$\bar{v}_3^B$	NIter	$\bar{v}_3^A$	$\bar{v}_3^B$	NIter
TMS4RD	Fail to converge			Fail to converge			Fail to converge		
TMS4RH	13.531	17.163	10	13.527	17.157	19	13.531	17.163	32
HS (TL) [7]	13.618	17.257	11	13.618	17.257	25	13.618	17.257	42

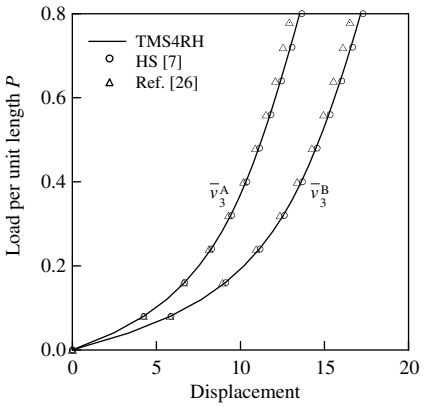

Fig. 9. Displacements of slit ring plate under line load.

the same mesh of the bilinear hybrid stress solid-shell elements. It should be noted that we derived the converged solutions for the TMS4RD element only in case of using NStep > 10.

5.1.4. Cylindrical shell with free edges

A cylindrical shell pulled by a pair of opposite concentrated forces is a very popular non-linear benchmark problem [7,12,26,27]. The geometrical and material data of the shell are given in Fig. 10.

Owing to symmetry of the problem, only one octant of the cylinder is discretized by the 8×16 mesh that was constructed by refining the 6×14 uniform mesh as shown in Fig. 10. Table 5 and Fig. 11 display a comparison of our results with results obtained by using identical or uniform 8×16 meshes of bilinear and 4×8 meshes of biquadratic solid-shell elements with the same node spacing. It is interesting that many

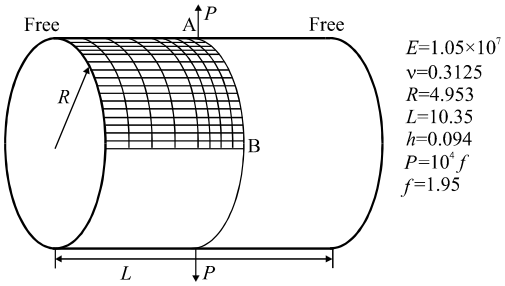

Fig. 10. Cylindrical shell with free edges.

Table 5
Transverse displacement under applied load of cylindrical shell with free edges

Element	NStep = 1		NStep = 5		NStep = 10	
	$\bar{v}_3$	NIter	$\bar{v}_3$	NIter	$\bar{v}_3$	NIter
TMS4RD	2.4337	23	2.4337	45	2.4337	61
TMS4RH	2.4337	8	2.4337	20	2.4337	33
HS (TL) [7][a]	2.4643	8	2.4643	22	2.4643	36
AS [12][a]	2.4537	9	2.4644	23	2.4648	37

[a] Results were obtained for loading factor $f = 2$.

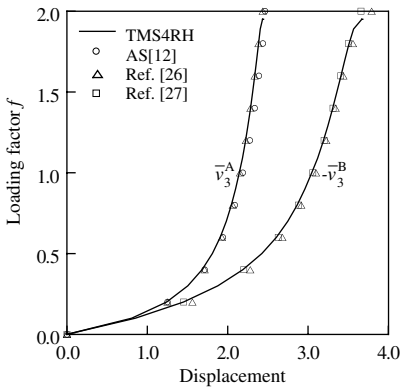

Fig. 11. Transverse displacements of cylindrical shell with free edges.

researchers detected a slight snap-through behaviour of the shell. So, Sze et al. [7] found that snap-through occurs when the loading factor f is between 1.9 and 2.0. Since we did not interest a post-buckling behaviour of the shell and taking into consideration the aforementioned result, we stopped our calculations at $f = 1.95$.

5.1.5. Pinched cross-ply hyperbolic shell

Further we consider a cross-ply hyperbolic shell under two pairs of opposite concentrated forces. The geometrical and material data of the three-layer hyperbolic shell are shown in Fig. 12, where 0° and 90° refer to the circumferential and meridional directions.

Due to symmetry of the problem, only one octant of the shell is modeled with the uniform 28×28 mesh of TMS4R elements. Table 6 and Fig. 13 display our results compared with those derived by Basar et al. [28] and Braun et al. [27] using the 28×28 mesh of bilinear and 14×14 mesh of biquadratic degenerated-shell and solid-shell elements, respectively, where $\bar{v}_x$ and $\bar{v}_y$ denote displacements of the middle surface in x and y directions. One may observe that the TMS4RH element performs excellently, since only seven iterations are needed to derive a converged solution for the [0/90/0] ply orientation.

5.2. Examples demonstrating advantages of Approach D

There were discovered only two benchmark problems exhibiting, on the contrary, the better convergence characteristics of Approach D, namely, a cantilever cross-ply semi-cylindrical shell and a 90° rigid-body rotation of one quarter of the circular ring.

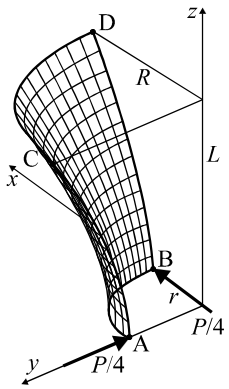

E_L=4×10^7
E_T=10^6
G_{LT}=G_{TT}=6×10^5
ν_{LT}=ν_{TT}=0.25
r=7.5
R=15
L=20
h=0.04
Ply thickness=h/3
P=40 f
f=10
Ply orientation=[0/90/0] and [90/0/90]

Fig. 12. Pinched cross-ply hyperbolic shell. Shell of revolution with geometrical parameters ($\alpha_1 = z \in [0, L]$, $\alpha_2 \in [0, \pi/2]$): $A_1 = \sqrt{1 + \dfrac{\mu^2 z^2}{A_2^2}}$, $A_2 = r\sqrt{1 + \dfrac{\mu z^2}{r^2}}$, $k_1 = -\dfrac{\mu r^2}{A_1^3 A_2^3}$, $k_2 = \dfrac{1}{A_1 A_2}$, $\mu = \dfrac{R^2 - r^2}{L^2}$.

Table 6
Displacements at points A and C of cross-ply hyperbolic shell

Ply sequence	Element	NStep = 1			NStep = 5			NStep = 10		
		$-\bar{v}_y^A$	$\bar{v}_y^C$	NIter	$-\bar{v}_y^A$	$\bar{v}_y^C$	NIter	$-\bar{v}_y^A$	$\bar{v}_y^C$	NIter
[0/90/0]	TMS4RD	Fail to converge			Fail to converge			3.5168	2.5185	56
	TMS4RH	3.5168	2.5185	7	3.5168	2.5185	16	3.5168	2.5185	27
[90/0/90]	TMS4RD	Fail to converge			Fail to converge			Fail to converge		
	TMS4RH	Fail to converge			6.0577	2.7291	24	6.0577	2.7291	36

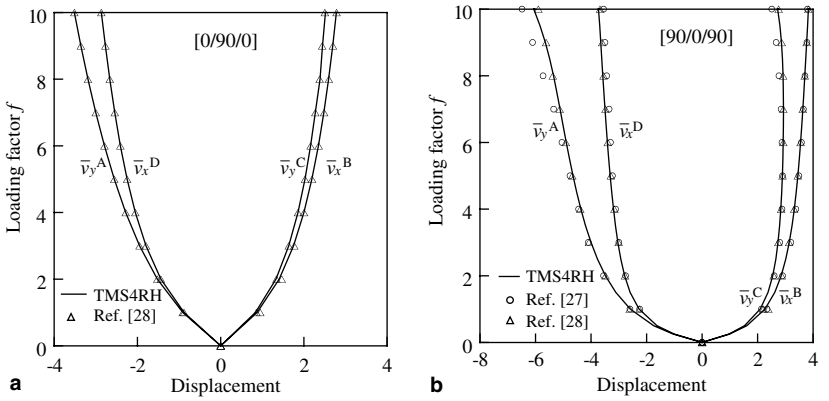

Fig. 13. Displacements of pinched cross-ply hyperbolic shell for ply orientations: (a) [0/90/0] and (b) [90/0/90].

5.2.1. Cantilever cross-ply semi-cylindrical shell under tip load

This problem has been used as a benchmark test for the non-linear behaviour of solid-shell elements in Refs. [6,7]. The geometrical and material data of the three-layer semi-cylindrical shell are given in Fig. 14, where R^{in} denotes the inner radius of the shell, subscripts L and T refer to the longitudinal and transverse directions of the individual ply, and 0° and 90° refer to the axial and circumferential directions of the cylinder.

Owing to symmetry of the problem, only half of the shell is discretized with the 16×16 mesh of TMS4R elements. Table 7 and Fig. 15 present our results compared with those reported in Refs. [6,7] by using the same mesh of the bilinear solid-shell elements. One may observe that the TMS4RD element performs

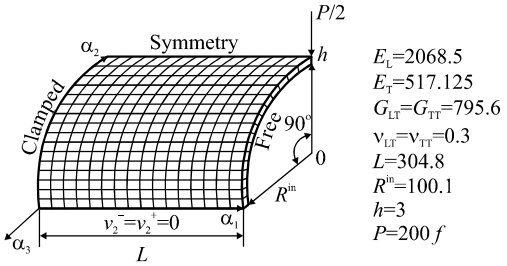

Fig. 14. Cantilever cross-ply semi-cylindrical shell under tip load. Ply thickness = 1, ply orientation = [90/0/90] and [0/90/0]. Shell of revolution with geometrical parameters: $A_1 = 1$, $A_2 = R^{in}$, $k_1 = 0$, $k_2 = 1/R^{in}$, $\alpha_1 \in [0, L]$, $\alpha_2 \in [0, \pi/2]$.

Table 7
Transverse displacement under applied load $f = 2.4$ of cantilever cross-ply semi-cylindrical shell

Ply sequence	Element	NStep = 1		NStep = 5		NStep = 10	
		$-\bar{v}_3$	NIter	$-\bar{v}_3$	NIter	$-\bar{v}_3$	NIter
[0/90/0]	TMS4RD	152.36	40	152.36	73	152.36	91
	TMS4RH	Fail to converge		Fail to converge		152.36	64
[90/0/90]	TMS4RD	74.120	19	74.120	38	74.120	54
	TMS4RH	Fail to converge		74.120	22	74.120	34

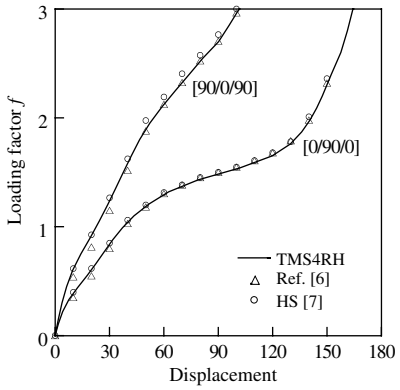

Fig. 15. Transverse displacement under applied load of cantilever cross-ply semi-cylindrical shell.

excellently. So, the TMS4RD solution converges for the [0/90/0] ply orientation in 40 iterations while TMS4RH and HS(TL) [7] solutions converge only in 64 and 68 iterations, correspondingly. Note that in Ref. [7] 150 units of the displacement under an applied load was prescribed in 10 equal increments.

5.2.2. 90° rigid-body rotation of one quarter of circular ring

The isotropic ring depicted in Fig. 16 is undergone 90° rigid-body rotation around point $\overline{M}$ belonging the midline $\overline{S}$. The geometrical and material properties of the problem are given in Fig. 16. The boundary conditions were taken as follows

$$u_1(M^{\pm}) = \mp h/2, \quad u_2(M^{\pm}) = 0, \quad u_3(M^{\pm}) = \mp h/2$$

and

$$u_1(L^{\pm}) = -2R \mp h/2, \quad u_2(L^{\pm}) = 0, \quad u_3(L^{\pm}) = \mp h/2.$$

One quarter of the ring is modeled by regular meshes of TMS4R elements. Table 8 lists strains at the central section (at $\alpha_1 = \pi R/4$) derived by using both elements developed. It is seen that the practically strain-free state is achieved by using eight TMS4RD elements. At the same time TMS4RH elements *never lead to* strain-free state at the central section of the ring. As we remember, the convergence tolerance was set to be 10^{-4}.

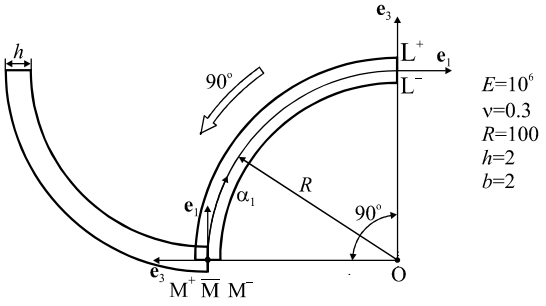

Fig. 16. 90° rigid-body rotation of one quarter of circular ring around point $\overline{M}$.

Table 8
Strains at central section (at $\alpha_1 = \pi R/4$) of one quarter of circular ring subjected to 90° rigid-body rotation

Element	Mesh	E_{11}^{-}	E_{11}^{+}	E_{13}^{-}	E_{13}^{+}	E_{33}	NIter
TMS4RD	2×1	1.22×10^{-1}	1.16×10^{-1}	5.34×10^{-2}	5.34×10^{-2}	-7.73×10^{-2}	8
TMS4RH	2×1	1.22×10^{-1}	1.16×10^{-1}	5.34×10^{-2}	5.34×10^{-2}	-7.73×10^{-2}	6
TMS4RD	4×1	1.81×10^{-2}	-5.12×10^{-3}	-8.63×10^{-3}	-8.69×10^{-3}	-5.86×10^{-5}	13
TMS4RH	4×1	5.90×10^{-2}	4.69×10^{-2}	1.09×10^{-1}	1.11×10^{-1}	-1.05×10^{-1}	22
TMS4RD	8×1	3.94×10^{-4}	-3.35×10^{-4}	6.76×10^{-6}	6.76×10^{-6}	-9.55×10^{-6}	31
TMS4RH	8×1	Fail to converge					

6. Conclusions

The geometrically exact TM shell FE models have been developed for the analysis of multilayered shells undergoing finite deformations. The FE formulation is based on the new non-linear strain–displacement relationships, written in local curvilinear coordinates, which are objective, i.e., invariant under all large rigid-body motions. The developed formulation has computational advantages compared to the conventional isoparametric FE formulations because displacement vectors of the face surfaces are introduced and resolved in the reference surface frame. An important observation is that our element stiffness matrices require only direct substitutions, i.e., no inversion is needed when sides of the element coincide with the lines of principal curvatures of the reference surface, and they are evaluated by using the analytical integration.

Two approaches for solving the incremental non-linear equilibrium equations are discussed in detail. In Approach D the incremental assumed strains and stress resultants are eliminated at the element level that practically leads to the displacement FE formulation. An alternative Approach H, in which equilibrium equations for incremental displacements and incremental assumed strains and stress resultants are solved by the Newton–Raphson method simultaneously, allows using much larger load increments. It should be mentioned that there were discovered two discriminating benchmark problems demonstrating, on the contrary, the better convergence characteristics of Approach D. It is important that corresponding D and H-element solutions (if they converge) yield *exactly* the same numerical results and all four-node elements developed are usually *insensitive* to a number of loading steps.

Acknowledgments

The present research was supported by Russian Fund of Basic Research (Grant No. 04-01-00070). Authors wish to thank the reviewer for his suggestion, which helped to improve a paper.

References

[1] G.M. Kulikov, S.V. Plotnikova, Non-conventional non-linear two-node hybrid stress–strain curved beam elements, Finite Elements Anal. Des. 40 (2004) 1333–1359.
[2] G.M. Kulikov, S.V. Plotnikova, Finite deformation plate theory and large rigid-body motions, Int. J. Non-Linear Mech. 39 (2004) 1093–1109.
[3] G.M. Kulikov, S.V. Plotnikova, Non-linear strain–displacement equations exactly representing large rigid-body motions. Part I. Timoshenko–Mindlin shell theory, Comput. Methods Appl. Mech. Engrg. 192 (2003) 851–875.
[4] H. Parisch, A continuum-based shell theory for non-linear applications, Int. J. Numer. Methods Engrg. 38 (1995) 1855–1883.
[5] R. Hauptmann, K. Schweizerhof, A systematic development of 'solid-shell' element formulations for linear and non-linear analyses employing only displacement degrees of freedom, Int. J. Numer. Methods Engrg. 42 (1998) 49–69.

[6] S. Klinkel, F. Gruttmann, W. Wagner, A continuum based three-dimensional shell element for laminated structures, Comput. Struct. 71 (1999) 43–62.
[7] K.Y. Sze, W.K. Chan, T.H.H. Pian, An eight-node hybrid-stress solid-shell element for geometric non-linear analysis of elastic shells, Int. J. Numer. Methods Engrg. 55 (2002) 853–878.
[8] J.C. Simo, M.S. Rifai, D.D. Fox, On a stress resultant geometrically exact shell model. Part IV. Variable thickness shells with through-the-thickness stretching, Comput. Methods Appl. Mech. Engrg. 81 (1990) 91–126.
[9] H.Y. Roh, M. Cho, The application of geometrically exact shell elements to B-spline surfaces, Comput. Methods Appl. Mech. Engrg. 193 (2004) 2261–2299.
[10] G. Wempner, D. Talaslidis, C.M. Hwang, A simple and efficient approximation of shells via finite quadrilateral elements, Trans. ASME J. Appl. Mech. 49 (1982) 115–120.
[11] Y.H. Kim, S.W. Lee, A solid element formulation for large deflection analysis of composite shell structures, Comput. Struct. 30 (1988) 269–274.
[12] H.C. Park, C. Cho, S.W. Lee, An efficient assumed strain element model with six dof per node for geometrically nonlinear shells, Int. J. Numer. Methods Engrg. 38 (1995) 4101–4122.
[13] K.Y. Sze, S. Yi, M.H. Tay, An explicit hybrid stabilized eighteen-node solid element for thin shell analysis, Int. J. Numer. Methods Engrg. 40 (1997) 1839–1856.
[14] G.M. Kulikov, S.V. Plotnikova, Simple and effective elements based upon Timoshenko–Mindlin shell theory, Comput. Methods Appl. Mech. Engrg. 191 (2002) 1173–1187.
[15] G.M. Kulikov, Non-linear analysis of multilayered shells under initial stress, Int. J. Non-Linear Mech. 36 (2001) 323–334.
[16] G.M. Kulikov, Analysis of initially stressed multilayered shells, Int. J. Solids Struct. 38 (2001) 4535–4555.
[17] S. Atluri, On the hybrid stress finite element model for incremental analysis of large deflection problems, Int. J. Solids Struct. 9 (1973) 1177–1191.
[18] P.L. Boland, T.H.H. Pian, Large deflection analysis of thin elastic structures by the assumed stress hybrid finite element method, Comput. Struct. 7 (1977) 1–12.
[19] C. Cho, S.W. Lee, On the assumed strain formulation for geometrically non-linear analysis, Finite Elements Anal. Des. 24 (1996) 31–47.
[20] A.L. Gol'denveiser, Theory of Elastic Thin Shells, Pergamon Press, Oxford, 1961.
[21] T.J.R. Hughes, T.E. Tezduyar, Finite elements based upon Mindlin plate theory with particular reference to the four-node bilinear isoparametric element, Trans. ASME J. Appl. Mech. 48 (1981) 587–596.
[22] K.J. Bathe, E.N. Dvorkin, A formulation of general shell elements—the use of mixed interpolation of tensorial components, Int. J. Numer. Methods Engrg. 22 (1986) 697–722.
[23] P. Betsch, E. Stein, An assumed strain approach avoiding artificial thickness straining for a nonlinear 4-node shell element, Commun. Numer. Methods Engrg. 11 (1995) 899–909.
[24] P. Betsch, F. Gruttmann, E. Stein, A 4-node finite shell element for the implementation of general hyperelastic 3D-elasticity at finite strains, Comput. Methods Appl. Mech. Engrg. 130 (1996) 57–79.
[25] Y. Basar, Y. Ding, Finite-rotation elements for the non-linear analysis of thin shell structures, Int. J. Solids Struct. 26 (1990) 83–97.
[26] C. Sansour, F.G. Kollmann, Families of 4-node and 9-node finite elements for a finite deformation shell theory. An assessment of hybrid stress, hybrid strain and enhanced strain elements, Comput. Mech. 24 (2000) 435–447.
[27] M. Braun, M. Bischoff, E. Ramm, Non-linear shell formulations for complete three-dimensional constitutive laws including composites and laminates, Comput. Mech. 15 (1994) 1–18.
[28] Y. Basar, Y. Ding, R. Schultz, Refined shear-deformation models for composite laminates with finite rotations, Int. J. Solids Struct. 30 (1993) 2611–2638.